ACS APPLIED MATERIALS & INTERFACES

Research Article

www.acsami.org

Graphene Oxide-Silver Nanocomposite: Novel Agricultural Antifungal Agent against *Fusarium graminearum* for Crop Disease Prevention

Juanni Chen,[†,‡] Long Sun,[†] Yuan Cheng,[†] Zhicheng Lu,[†] Kang Shao,[†] Tingting Li,[†] Chao Hu,[†] and Heyou Han*[,†]

[†]State Key Laboratory of Agricultural Microbiology, College of Plant Science and Technology, College of Science, Huazhong Agricultural University, Wuhan, 430070, P.R. China

[‡]Laboratory of Natural Product Pesticide, College of Plant Protection, Southwest University, Chongqing, 400715, P.R. China

Supporting Information

ABSTRACT: Nanoparticle-based antibacterial agents have emerged as an interdisciplinary field involving medicine, material science, biology, and chemistry because of their size-dependent qualities, high surface-to-volume ratio, and unique physiochemical properties. Some of them have shown great promise for their application in plant protection and nutrition. Here, GO-AgNPs nanocomposite was fabricated through interfacial electrostatic self-assembly and its antifungal activity against phytopathogen *Fusarium graminearum* was investigated in vitro and in vivo for the first time. The results demonstrated that the GO-AgNPs nanocomposite showed almost a 3- and 7-fold increase of inhibition efficiency over pure AgNPs and GO suspension, respectively. The spore germination inhibition was stimulated by a relatively low concentration of 4.68 μg/mL (minimum inhibition concentration (MIC)). The spores and hyphae were damaged, which might be caused by an antibacterial mechanism from the remarkable synergistic effect of GO-AgNPs, inducing physical injury and chemical reactive oxygen species generation. More importantly, the chemical reduction of GO mediated by fungal spores was possibly contributed to the high antimicrobial activity of GO-AgNPs. Furthermore, the GO-AgNPs nanocomposite showed a significant effect in controlling the leaf spot disease infected by *F. graminearum* in the detached leaf experiment. All the results from this research suggest that the GO-AgNPs nanocomposite developed in this work has the potential as a promising material for the development of novel antimicrobial agents against pathogenic fungi or bacteria.

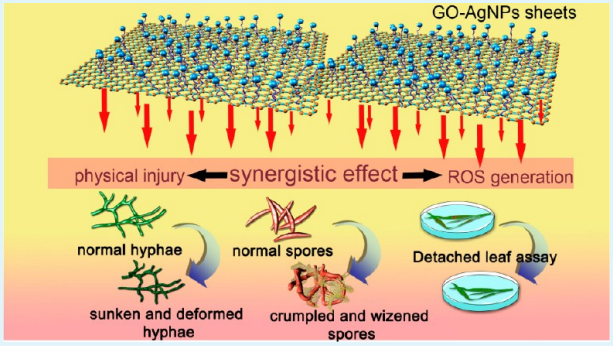

KEYWORDS: *GO-AgNPs nanocomposite, Fusarium graminearum, antifungal activity, synergistic effect, detached leaf experiment*

1. INTRODUCTION

Fusarium is a complex and multiple species of fungal phytopathogen, causing fargoing and catastrophic diseases of most cultivated crops, such as Fusarium head blight (FHB) of wheat and barley and crown rot (CR) of maize, all of which can tremendously reduce the crop quality and yield.[1] Besides, during the infection process, several secondary metabolites (mycotoxins), including trichothecene deoxynivalenol (DON), are produced by the pathogenic fungi.[2] These mycotoxins, functioning as a virulence factor, accelerate the aggressiveness of pathogen to host plants and their residues on contaminated grains, if consumed, are detrimental to human and animal health.[2]

Conventionally, the measurement strategy for plant fungal disease prevention and control mainly depends on the use of chemical agents.[1] Unfortunately, indiscriminate use of bactericides has brought some thorny environmental problems. Biological control has also been developed for therapeutic applications (field management). Previous studies found that *Fusarium* wilts (of cucumber and flax) could be suppressed through the application of fluorescent *Pseudomonas spp.* stains and *Streptomyced sp.* strains, and the mechanism is attributed to the production of chitinolytic enzymes.[3] But their practical applications are restricted by variable environmental factors, resulting in inadequate distribution. Antifungal peptide (AFP) genes and engineered proteins have been expressed in plants through genetic engineering to enhance their resistance to the pathogens.[4,5] This approach to disease management may not be readily available since pathogens too tend to evolve virulent variants. In this case, it is essential to develop an innovative and effective alternative to maintain a sustainable balance of complementary approaches for disease control.

Currently, the rapid growth in nanotechnology is increasing the likelihood of combining engineered nanomaterials with

Received: May 19, 2016
Accepted: August 26, 2016
Published: August 26, 2016

ACS Publications © 2016 American Chemical Society

DOI: 10.1021/acsami.6b05730
ACS Appl. Mater. Interfaces 2016, 8, 24057−24070

biotechnology to expand the application domain of nanomaterials. In particular, to our best knowledge, a variety of nanomaterials have been developed into novel antimicrobial agents for agricultural disease control, including TiO_2[6] and AgNPs.[7,8] Carbon-based nanomaterials are particularly interesting because of their extremely high mechanical strength and prominent physicochemical properties in interaction with bacteria. Previous findings have suggested that various nanomaterials, like graphene oxide (GO), reduced graphene oxide (RGO), SWCNT, MWCNT and C60, exhibited strong antimicrobial activity against phytopathogen,[9,10] fungi and cells.[11]

Silver nanoparticles (AgNPs), as reported with excellent toxicity to a wide range of microorganisms, are the most extensively studied and have been applied in the medicine field for treating a variety of infections and synthesizing composites or manufacturing medical devices used as antibacterial agents.[12,13] Moreover, they revealed mild toxicity toward human cells at an extremely low concentration.[14] Various studies have demonstrated that the bactericidal effect of AgNPs is closely related with their size,[15] shape,[16] surface chemistry,[17] stability,[18] and surface charge.[19] Nevertheless, commercially available bare AgNPs with high reactivity lead to particle aggregation and settling, prompting the decrease of antibacterial activity.[20] Thus, various organic[21] and inorganic[22] substances are used to stabilize AgNPs or to control the release of silver ion. Graphene oxide, a single-atom-thick and two-dimensional (2D) sp^2-bonded carbon honeycomb lattice, has been functionalized miscellaneously, because of its intriguing surface chemical properties, especially the large surface area[23] and high water solubility of GO nanosheets.[24] GO is also increasingly considered as an eminent support material which can be hybridized with DNA,[25] metal oxides,[26] polymers[27] and inorganic nanoparticles.[28] Additionally, various graphene-based components have been used as antibacterial agents, even in antiviral applications. For example, graphene oxide-TiO_2 thin films were applied as nanocomposite photocatalysts for degradation of *Escherichia coli* (*E. coli*) in solar light irradiation, resulting in a 7.5-fold improvement of the antibacterial activity of the TiO_2 thin film.[29] Graphene-tungsten oxide composite also exhibited photoinactivation which can cause protein degradation and RNA efflux of bacteriophage MS2 viruses under visible light irradiation.[30] Recently, Hu et al. have obtained stabilized RGO-AgNPs hybrids using the simple one-pot boiling method.[31] The nanocomposite possesses better dispersibility owing to abundant hydroxyl and carboxyl groups located at the edges of GO. In addition, GO sheets can also act as bridges to bind silver nanoparticles homogeneously to prevent them from agglomeration and then lead to enhanced antibacterial activity toward *E. coli*.[32] As a novel efficient nanobactericide, GO sheets and silver nanoparticles have been reported to possess broad-spectrum antimicrobial activity against phytopathogens in vitro and have significant effect in the control of plant disease by field experiment.[7,9,33] However, little is known about whether the GO-AgNPs nanocomposite has antifungal activity toward fungal pathogens.

In the present study, GO-AgNPs nanocomposite was fabricated through interfacial electrostatic self-assembly and we investigated, for the first time, the sporicidal activity and antifungal activity of the GO-AgNPs nanocomposite against typical *F. graminearum* that causes FHB disease in wheat plants. The results showed that GO-AgNPs nanocomposite displayed a high inactivation rate of conidia of *F. graminearum*. The spore germination was significantly inhibited compared with Ag nanoparticles and GO sheets alone. Moreover, the effects of these nanomaterials on the hyphae and their practical applications conducted on detached-leaves were also investigated. Considering the novel and high antifungal activity at such a low concentration (7.81 μg/mL), the GO-AgNPs nanocomposite has good biocompatibility and can be used as a promising material for prevention of pathogenic fungal or bacterial infections in crop protection.

2. MATERIALS AND METHODS

2.1. Chemicals and Reagents. Graphite powder (99.99%), silver nitrate ($AgNO_3$), 1% sodium citrate dihydrate, sodium borohydride ($NaBH_4$), potato dextrose agar (PDA) medium, polyvinylpyrrolidone (PVP), poly dimethyl diallyl ammonium chloride (PDDA), and carboxy methylated cellulose(CMC) were purchased from Sigma-Aldrich. The microbes were obtained from the State Key Laboratory of Agricultural Microbiology of Huazhong Agricultural University (Wuhan, China).

2.2. Synthesis of Graphene Oxide and AgNPs Using the Chemical Reduction Method. GO nanosheets were prepared as described previously.[34] GO was prepared from natural graphite powders by the modified Hummers method.[34] Briefly, the natural graphite powders (99.99%; Sigma-Aldrich) were initially oxidized by concentrated sulfuric acid (H_2SO_4) to produce graphite oxide (GtO). After filtering and washing with deionized water to remove chemical residues, the GtO was dispersed in deionized water and bath-sonicated (Elamsonic, S60H) for 3 h to exfoliate the GO mixture (GO).

AgNPs were prepared based on a typical procedure.[35] AgNPs were obtained by reducing $AgNO_3$ with $NaBH_4$ in water suspension using citrate as stabilizing agent. Specifically, 5 mL of 10 mM was mixed with 45 mL of ultrapure water at 45 °C and heated rapidly to boiling. Then 1 mL of 1% sodium citrate dihydrate and 300 μL of 3 mM $NaBH_4$ were injected dropwise under vigorous stirring and the resulting solution was kept at boiling temperature for 60 min. After cooling to room temperature, the solution was filtered through a polycarbonate membrane (0.22 μm). The final mixture was centrifuged at 8000 rpm and the pellets were resuspended in water. The concentration of resultant AgNPs was 0.1 mg/mL.

2.3. Synthesis of GO-AgNPs Nanocomposite by Electrostatic Self-Assembly. Graphene oxide was exfoliated by ultrasonication in water for 2 h to obtain the aqueous homogeneous graphene oxide dispersion (1.0 mg/mL). PVP-capped graphene oxide was first prepared by mixing 80 mg of PVP with 20 mL of 0.25 mg/mL graphene oxide solution, followed by stirring for 30 min. The mixture was washed at least three times by centrifugation and then suspended in 5 mL of water. Next, 0.1 mL of 20 wt % PDDA was mixed well with 16.8 mL of 0.625 M KCl, followed by injecting 4.2 mL of PVP-capped graphene oxide to get PDDA-functionalized graphene oxide (PDDA-GO). The resulting solution was sonicated for 1.5 h, followed by washing and centrifugation three times. Finally, the PDDA-GO was redispersed in 4 mL of water, forming a clear and brownish yellow suspension with a final concentration of 1.0 mg mL^{-1}.

The GO-Ag composites were synthesized based on a previous method.[36] Forty microliters of 1.0 mg/mL PDDA-GO were added to 1.5 mL of as-prepared AgNPs under stirring. Then the solution was sonicated for 3 min before standing overnight. The precipitate was washed several times and freeze-

DOI: 10.1021/acsami.6b05730
ACS Appl. Mater. Interfaces 2016, 8, 24057−24070

dried before redispersion in 1 mL of deionized water for further use.

2.4. Characterization of GO-Ag Nanocomposite. The UV−vis absorption spectra were confirmed using a Shimadzu UV-1650PC spectrometer to detect the presence of AgNPs and GO sheets. The morphology of the as-prepared nanoparticles was observed by transmission electron microscopy (TEM). The nanocomposite suspensions (10 μL) were dropped on carbon-coated copper grids and air-dried for TEM analysis. TEM measurements were performed by Hitachi H-7650 EM with an accelerating voltage of 300 kV. X-ray diffraction (XRD) was carried out to analyze the crystallographic structure using a Rigaku D/MAX-rA diffractometer with Cu Kα radiation (λ = 1.5406 Å). X-ray photoelectron spectroscopy (XPS) measurements were conducted on a Thermo VG Multilb 2000 spectrometer equipped with a monochromatic Al Kα radiation source. Raman spectra were collected with a Renishaw inVia model confocal microscopy Raman spectrometer (Renishaw, UK) at an excitation wavelength of 633 nm. Both Zeta-potential and dynamic light scattering were measured with a Zetasizer Nano ZS (Malvern Instruments, England).

2.5. Cells Culture. The representative wheat pathogen *F. graminearum* was purchased from the State Key Laboratory of Agricultural Microbiology of Huazhong Agricultural University (Wuhan, China).

F. graminearum, one kind of filamentous pathogenic fungi, was maintained on Difco-Bacto Potato Dextrose Agar (PDA) at 28 °C. After 5 days of incubation in an incubator, *F. graminearum* spores were obtained as described previously.[37] The mycelia of *F. graminearum* were incubated in CMC liquid medium for 5 days under light conditions with gentle shaking to obtain macroconidial suspensions. After filtering the suspensions through sterilized gauze, the conidia were harvested by centrifugation at 3,500 rpm for 5 min and washed twice with sterile distilled water. The spore suspensions were first adjusted to a desired concentration of 3×10^7 spores per mL. All experiments were carried out in triplicate at room temperature.

2.6. In Vitro Investigation of Antifungal Activity. To investigate the antifungal activity of the synthesized nanocomposites against phytopathogen, the synthesized bare AgNPs, GO, and GO-AgNPs nanocomposite were studied separately. The fungistatic and fungicidal activities of GO, AgNPs, and GO-AgNPs nanocomposite were investigated by the modified microdilution method to determine the minimum inhibitory concentration (MIC) and minimum fungicidal concentration (MFC). In a preliminary experiment, the dispersion of GO-AgNPs hybrids was diluted in a geometric progression from 2 to 64 times (in the concentration range of 125−3.90 μg/mL) and the obvious concentration range of GO-AgNPs nanocomposite tested in this experiment was between 15.62 and 7.81 μg/mL (Figure S2). After diluting the initial dispersion (15.62 μg/mL) by 1, 0.9, 0.8, 0.7, 0.6, and 0.5 times, the obtained concentrations of GO-AgNPs nanocomposite decreased gradually from 15.62 to 7.81 μg/mL (15.62, 14.06, 12.5, 10.93, 9.37, 7.81 μg/mL). The MIC value is defined as the lowest concentration of GO-AgNPs at which the visible growth of microorganisms was significantly inhibited compared with the blank. For spore germination inhibition test, *F. graminearum* spores were prepared as described previously.[37] Briefly, 100 μL aliquots of spore suspensions (3×10^7 spores mL^{-1}) were mixed with 100 μL of GO-AgNPs nanocomposite in the tubes to obtain a final concentration of 3.9, 4.68, 5.46, 6.25, 7.03, and 7.81 μg/mL. Then, 50 μL of the mixture was pipetted onto sterile concave slides. After incubation at 28 °C for 7 h, at least two hundred spores per treatment were assessed by measuring the germination rates, and comparing them to those of the control samples containing spore suspensions and 20 μL of deionized water. The spore germination rate was calculated as follows: spore germination rate (%) = (the number of germinated spores)/(total number of spores).

The high humidity level was maintained during germination. Three concave slides were prepared for all treatments and repeated at least three times. Meanwhile, micrographs were taken with a digital camera connected to a Leica microscope (Germany DCF425).

The cell viability of *F. graminearum* spores mixed with GO-AgNPs hybrids was determined by the standardized colony forming units (CFU) counting. Briefly, after 3 h incubation of inoculum suspensions and nanocomposite, gradient-diluted samples were transferred onto their respective potato dextrose agar plates, cultured at 30 °C for 3 days, and spotted until growth was observed in the control plates. Finally, the colonies of cells were counted. The concentration in the treated samples with no growth of colonies or fewer than three colonies (approximately 99 to 99.5% killing activity) was recorded as the minimum fungicidal concentration (MFC). Meanwhile, the comparison experiments were conducted to examine the fungistatic and fungicidal activities of AgNPs and GO sheets separately.

2.7. Morphological Analysis of Fungal Hyphae. SEM was used to examine morphological changes of *F. graminearum* hyphae with and without the treatment of GO-AgNPs nanocomposite.[10] After blank PDA plates were prepared, several cellophane membranes were sterilized by boiling in distilled water and then placed on the surface of the agar plates. A fungal cake was cut from the 5-day-old *F. graminearum* grown on PDA medium and then placed at the center of the agar plates covered with the cellophane membranes. All the plates were incubated in a humid chamber at 28 °C for 3 days, and then the fungal culture was sprayed with 2 mL of GO-AgNPs nanocomposite for 3 days, followed by another 3 days of incubation. DI water was applied for the control group. Three days later, the cellophane membranes were removed from the agar, and the hyphal structure was observed and photographed under an optical microscope in vivo. Additionally, pieces of mycelial material were cut from the edge of the fungal cultures, fixed with 2.5% glutaraldehyde, postfixed with 1% aqueous OsO4 (Fluka) and washed with 0.1M, pH 7.0 phosphate buffers. Subsequently, the samples were dehydrated separately in an ascending ethanol series (30, 50, 70, 80, 90, and 100%) for 15 min, and dried in a vacuum oven. Finally, thin sections containing the cells were placed on the copper grids and observed under a SEM (JEOL JSM-6700F).

2.8. Spore Observation by SEM and TEM. The morphological changes of spores were further investigated using SEM and TEM after treatment with GO-AgNPs nanocomposite.[10] The bacterial suspensions were treated with GO-AgNPs for 2 h at 30 °C and the spore suspensions were treated with GO for 3 h at 28 °C. After centrifugation at 6000 rpm for the bacterial cells and 3500 rpm for the conidia, the condensed cells were fixed with 2.5% glutaraldehyde, postfixed with 1% aqueous OsO_4 (Fluka) and washed with 0.1 M, pH 7.0 phosphate buffer. Then, the samples were dehydrated separately in an ascending ethanol series (30, 50, 70, 80, 90 and 100%) for 15 min, and dried in a vacuum oven. Finally,

DOI: 10.1021/acsami.6b05730
ACS Appl. Mater. Interfaces 2016, 8, 24057−24070

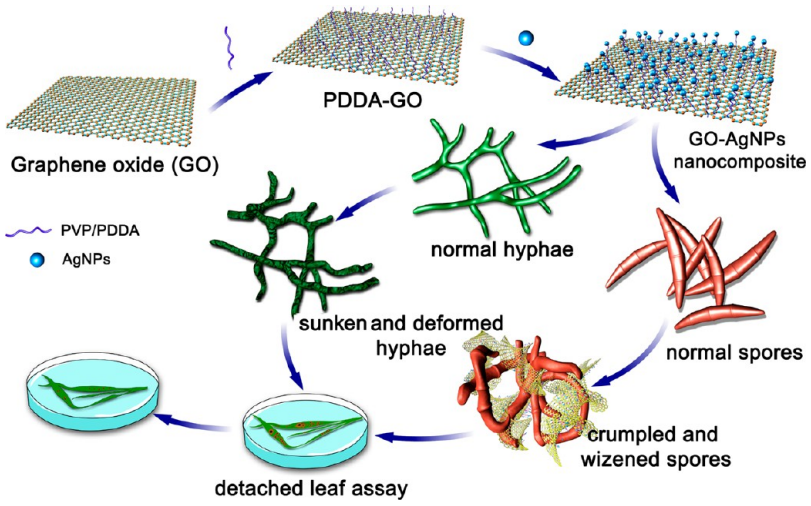

Figure 1. Schematic illustration of fabrication of GO-AgNPs nanocomposite and its antifungal characterization in vitro and in vivo.

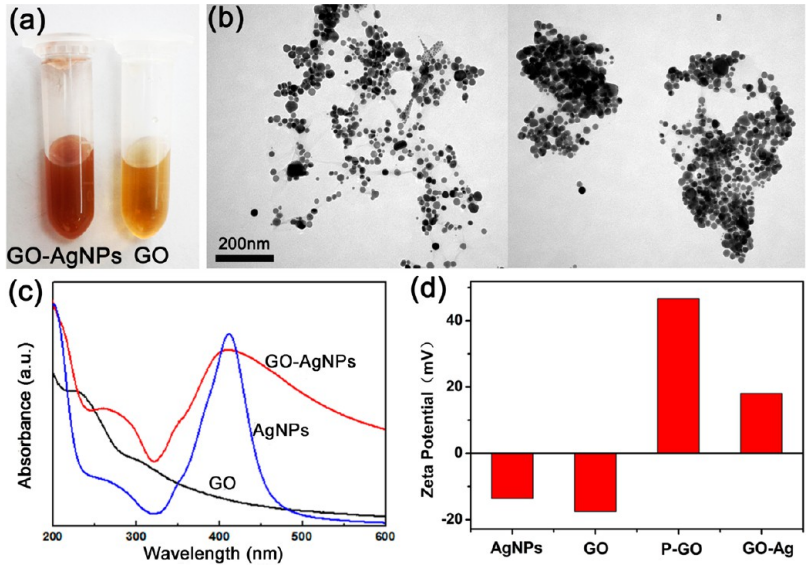

Figure 2. Synthesis and characterization of GO-AgNPs nanocomposite. (a) Light photo of GO sheets and GO-AgNPs nanocomposite dispersed in DI water, (b) TEM images of GO-AgNPs hybrids, (c) UV−vis absorption spectra, and (d) zeta potential of AgNPs, GO sheets, P-GO, and GO-AgNPs nanocomposite.

thin sections containing the cells were placed on the copper grids and observed under a SEM (JEOL JSM-6700F) and TEM microscope (FEI, Czech).

2.9. Reactive Oxygen Species (ROS) Assay. The production of ROS in fungal spores induced by nanomaterials can be measured. Here, we focused on an assay to detect the ROS level using reactive oxygen species assay kit, which mainly contained nonfluorescent molecule 2′,7′-dichlorodihydrofluorescein diacetate (DCFH-DA). After deacetylation to 2′,7′-dichlorodihydrofluorescein (DCFH) by intracellular esterases, DCFH was oxidized by intracellular ROS to yield fluorescent dichloroflurescein (DCF).[9] Briefly, spore cells (~10^5 per mL) were incubated with 200 μL of GO, AgNPs and GO-AgNPs for 2h at 30 °C, and then, the cells were washed three times with 0.1 M PBS(PH 7.8) and resuspended in PBS solution. As a positive control, the spores were treated with sterilized water. Two microliters of DCFH-DA (30 μM) was added to the cell suspension and cultured for another 1h in complete darkness. The fluorescence intensity was measured on an Edinburgh FLS920 spectrometer at 522 nm.[9] The level of intracellular ROS was expressed as the ratio of fluorescence intensity of each sample to the intensity of a control sample.

2.10. Silver Ion Release Property. The property of sliver ion release (from AgNPs surfaces) of the GO-AgNPs nanocomposite was studied by dialysis experiment. In the experiment, a dialysis tube (cellulose ester; MWCO 100 000 Da) made of a semipermeable membrane was filled with 5 mL nanocomposite dispersion of a certain concentration and immersed in 100 mL of ultrapure water. Under mild and continuous stirring at 30 °C for 10 days, the ultrapure water was changed every day to collect samples at different time points. All the obtained samples containing released silver ion was analyzed by inductively coupled plasma atomic emission spectrometry (ICP-AES, IRIS Advantage ER/S)

2.11. Plant Growth Conditions and Phytopathogen Inoculation in Detached Leaf Assay. The wheat seeds were purchased from a local seed company. Wheat seeds were germinated in the 30 cm^2 plastic pots containing a mixture of

DOI: 10.1021/acsami.6b05730
ACS Appl. Mater. Interfaces 2016, 8, 24057−24070

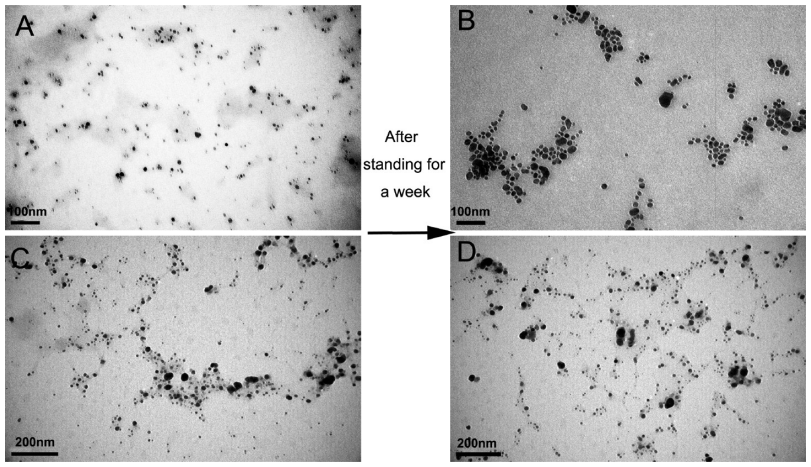

Figure 3. TEM images of synthesized AgNPs (A), AgNPs after standing for a week (B), GO-AgNPs nanocomposite (C) and GO-AgNPs nanocomposite after standing for a week (D).

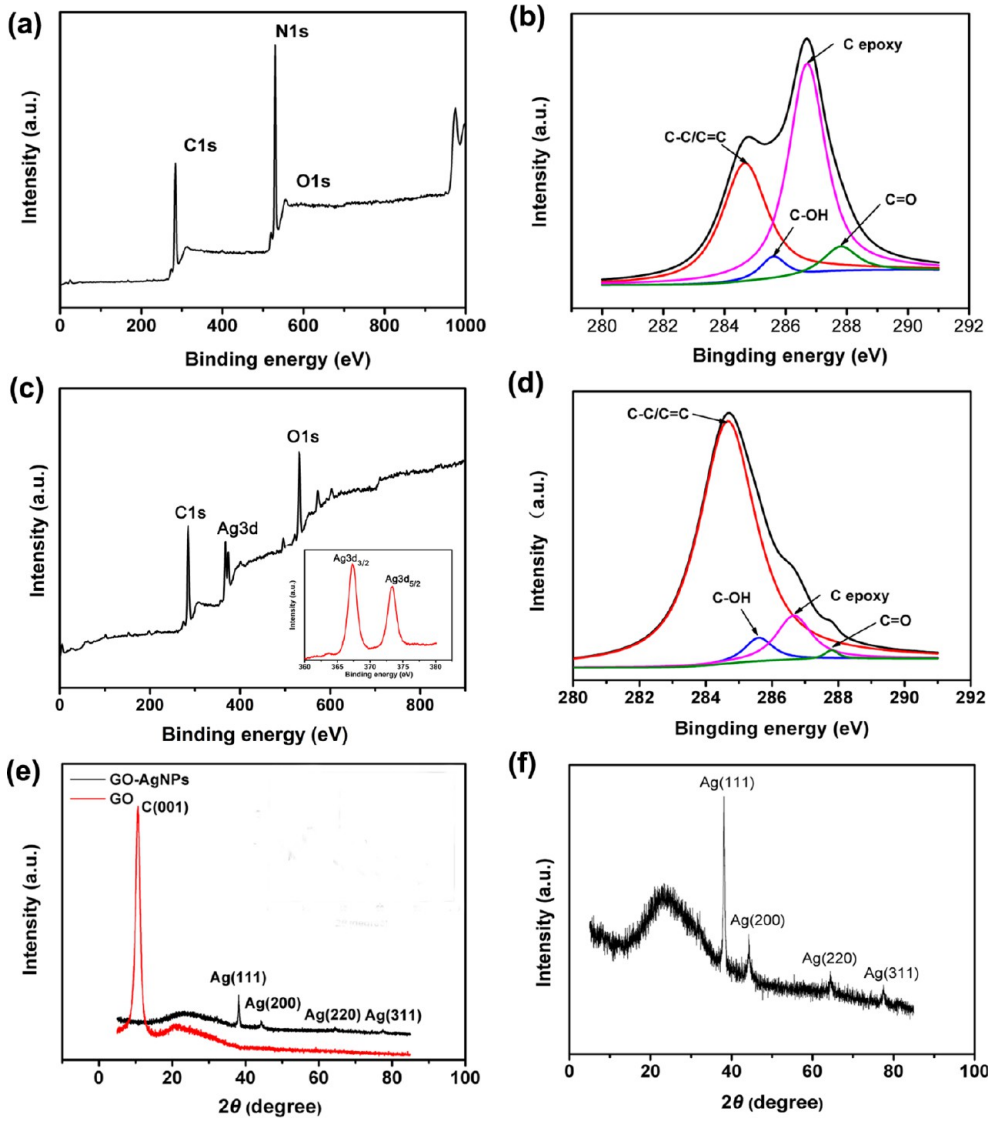

Figure 4. XPS profiles of (a) GO sheets, (b) peak deconvolution of C 1s spectra, (c) GO-AgNPs nanocomposite (inset is Ag 3d spectra), and (d) C 1s spectra. (e) XRD patterns of GO-AgNPs and GO and (f) crystallographic planes of AgNPs.

nutritional soil, with 10 seeds per pot and 1 cm or a larger distance between each seed. All the pots were arranged at random in triplicate in a growth chamber and maintained at 24 ± 1 °C with 40 ± 10% relative humidity and 14-h photoperiod

DOI: 10.1021/acsami.6b05730
ACS Appl. Mater. Interfaces 2016, 8, 24057−24070

for 3 weeks before use for experiment. Then, the seedlings were harvested and 5 cm long segments were cut from the leaf and inserted into the 0.5% water agar containing 10 mg/L kinetin as preservative.[38]

For the phytopathogen inoculation in vivo, two leaves were pierced from the wheat plants per pot at the center of the adaxial surface using a sterile needle and inoculated with 10 μL of the as-prepared *F. graminearum* conidial suspension through the micropores at three inoculation points between the leaf veins, followed by incubation of the wheat leaves at 28 °C under continuous light condition.[39] During incubation, 7.81 μg/mL of GO-AgNPs nanocomposite was sprayed on the wheat leaves every day and sterilized distilled water was used for the control group. A total of ten leaves were used for every treatment and the lesion size was measured as the indicator of pathogen aggressiveness after 1 week.

2.12. Statistic Analysis. All the experiments were performed in triplicate and the results were expressed as mean ± SD (standard deviation). Statistical analysis was performed using Statistical Product and Service Solutions Software (SPSS 11.0, United States). The differences between the groups were assessed using the analysis of variance test. The results were considered statistically significant at $P < 0.05$ or 0.01.

3. RESULTS AND DISCUSSION

3.1. Characterization of the GO-Ag Nanocomposite. In this experiment, as shown in the schematic illustration in Figure 1, the GO-AgNPs nanocomposite (or other hybrids) was formed using an electrostatic self-assembly strategy.[36] GO and AgNPs were separately synthesized, and then GO was modified with poly(diallyldimethylammonium chloride) (PDDA) capped on the surface as surfactant to obtain the positive potential-functionalized graphene oxide (PDDA-GO). The PDDA-GO can promote the loading of the negatively charged Ag nanoparticle. Finally, the nanocomposite was freeze-dried for further analysis. Zeta-potential was measured to verify the electrostatic interaction. As shown in Figure 2, the mean zeta potential of the GO sheets was negative due to the abundant oxygen-containing groups (carboxy group and hydroxyl). Then PDDA-functionalized GO exhibited a positive charge of 33 mV after modification with PDDA. When added into the dispersion of PDDA-GO sheets, the negative-charged AgNPs (−19.3 mV) were assembled on the surface of PDDA-GO via electrostatic interaction to obtain GO-Ag nanocomposite with positive surface charge. Therefore, PDDA is likely to play a significant role in the formation of GO-AgNPs nanocomposite.

For silver nanoparticle alone, there is strong dispersion difficulty because of its strong adhesion forces between particles with high surface energy.[40] Graphene oxide can attach metal nanoparticles onto the hyphal interfaces, as a kind of dispersion and surfactant-like agent.[41] A previous investigation has proved that graphenelike carbon shell facilitated the dispersion of metals in polymers by mechanically entrapping metal nanoparticles, which was possibly attributed to the covalent and chemical functionalization of metal particles.[42]

The loading of AgNPs onto the GO sheets was characterized by TEM and several other techniques. The TEM image shown in Figure 2b is a representative micrograph of GO-AgNPs nanocomposite. The whole single GO sheets could be seen to be filled with plenty of AgNPs, and some areas were overlapped with AgNPs with a darker color, demonstrating that the AgNPs were homogeneously attached to the surface of GO sheets and the particle diameters were roughly in the range of 10 to 35 nm. As shown in Figure. 3, after standing for a week, the AgNPs suspension became concentrated while GO-AgNPs nanocomposite was well distributed at a much higher concentration (20 μg/mL) compared to the newly synthesized products. According to the results in our experiment, GO obviously altered the charge and aggregation behavior of AgNPs, thus effectively enhancing the dispersion state of the nanoparticle. The UV absorption peak of typical sliver nanoparticles was at around 410 nm. After attachment to GO sheets, the absorption spectra of GO-AgNPs hybrids showed a significant shift to 450 nm compared with the characteristic absorption peak of GO at 230 nm, which was attributed to a surface plasmon, indicating large amounts of AgNPs were successfully loaded on the GO sheets.[43]

The X-ray diffraction (XRD) patterns and X-ray photoelectron spectra (XPS) were also collected to confirm the presence of Ag nanopaticle. As shown in Figure 4e, a sharp peak at $2\theta = 10.5°$ could be observed for GO sheets, which was assigned to the (001) reflection of GO. However, the peak of GO sheet, probably attributed to the interlamellar water trapped between hydrophilic GO sheets at 2θ value around 10.5°, completely disappeared after electrical decoration with AgNPs. Additionally, intensive peaks appeared at 2θ value of 38.1, 44.3, 64.2, and 77.6°, which were assigned to the (111), (200), (220), and (311) crystallographic planes of face-centered-cubic Ag nanoparticles, respectively (JCPDS No. 07-0783).[44] X-ray photoelectron spectrum (XPS) was also used to analyze the chemical structure of the hybrid. As shown in Figure 4a, the C 1s XPS spectrum of GO clearly displayed the oxidation with five components that corresponded to carbon atoms in different functional groups: C−C/C═C (284.8 eV), C−OH (285.8 eV), C (epoxy) (286.7 eV), and C═O (287.8 eV), indicating the successful synthesis of GO sheets. After reduction with sodium citrate, the peak intensity assigned to oxygen-containing functional groups was obviously decreased when compared with the samples of pure GO sheets (Figure 4c). An additional Ag 3d peak appeared in GO-AgNPs nanocomposite relative to the samples of pure GO sheets, indicating the changes of the surface composition (Figure 4c). The incisive peaks with binding energies at 368.1 and 374.1 eV in the Ag 3d core-level XPS spectrum were ascribed to Ag 3d3/2 and Ag 3d5/2 photoelectrons, respectively. This observation is in agreement with a previous study.[45] In particular, the C 1s (binding energy at 284.7 eV) and O 1s (binding energy at 531.7 eV) in the XPS spectrum could still be observed when GO was functionalized, implying that the residual oxygenated groups on the surface of GO sheets could enable the composites to be well dispersed, as shown in Figure 2b.[44]

Raman spectra, which are usually used for structural and electronic characterization of graphitic materials, were also measured at room temperature using a Raman microspectrometer (Renishaw, UK) at an excitation wavelength of 633 nm. To analyze the properties of single-, double-, and multilayer graphene oxides, we measured the variation of the 2D band of Raman spectra. As presented in Figure S1a, the representative disordered D and G bands of GO sheets were clearly observed at nearly 1350 and 1585 cm^{-1}, respectively, which were attributed to the in-plane *A1g* (LA) zone-edge mode and the *E2g* mode, resulting from the significant amorphization of graphite lattice as amorphous carbon contained a certain fraction of sp^3 carbons.[46] In TEM, the

DOI: 10.1021/acsami.6b05730
ACS Appl. Mater. Interfaces 2016, 8, 24057−24070

single-layer GO sheets could be observed, but the Raman characteristic was not detected, probably due to the difference in detection methods. The 2D/G ratios typically reached 0.81or 0.32, indicating the presence of double thin film and triple-layers along with some wrinkles at the edges, which was consistent with a previous study.[47] The 2D band appeared approximately at 2659 cm^{-1}. For triple-layer GO sheets, the G and 2D spectrum variation occurred at 1586 and 2673 cm^{-1}, respectively. Triple-layer GO exhibited a higher D/G ratio (1.38) than the double-layer (0.82), which was attributed to the edge defects of overlapping region.[47] In the case of Raman spectrum of GO-AgNPs (Figure S1c), many primary vibration bands were observed, including higher intensive G and D bands at 1356 and 1595 cm^{-1}, due to surface enhanced Raman scattering (SERS) effect of AgNPs deposited on GO sheet surface.[48] These results also displayed the presence of graphene oxide. The peaks at 1021 and 1069 cm^{-1} were assigned to CH deformation and the ring breathing modes, respectively, and the bands at 1595 and 1606 cm^{-1} were ascribed to the C=C stretching vibration mode.

3.2. Fungistatic and Fungicidal Activities of GO-Ag Nanocomposite. The antifungal activity of self-assembled GO-AgNPs nanocomposite against *F. graminearum* was investigated in comparison to that of AgNPs and GO sheets. The fungistatic activity was confirmed by the microdilution method. Just like silver NPs, the MIC of GO-AgNPs nanocomposite against the tested spores was as low as 4.68 μg/mL (Table 1), revealing its brilliant antifungal properties.

Table 1. MIC and MFC of GO-AgNPs Nanocomposite against *F. graminearum* Spores[a]

	MIC			MFC		
tested fungi	AgNPs	GO-AgNPs	GO	AgNPs	GO-AgNPs	GO
F. graminearum	4.68	4.68	50	12.5	9.37	500

[a]The results were obtained from experiments repeated at least three times.

Previous research found that the as-prepared GO with an average lateral dimension of 11 ± 4 nm exhibited cytotoxic effects only at up to 10 μg/mL, while the sheets could significantly destroy the cell at 100 μg/mL.[49] The low concentration advantage of GO-AgNPs is extraordinarily conducive to their promising application in vivo. From Figure 5, it can be seen that, after incubation with GO-AgNPs dispersion and AgNPs, the germination rate of spores was gradually decreased with an increase of their concentrations. However, PVP and PDDA cannot produce any effect on the spore growth (Figure 5b and Figure S2).

Interestingly, AgNPs exhibited a slightly higher but not statistically significant antibacterial activity relative to GO-AgNPs nanocomposite in the concentration range of 3.9−5.46 μg/mL. The increased concentration witnessed a sharp drop of the germination rate to 11.38% for the GO-AgNPs nanocomposite at 7.81 μg/mL, but a moderate decrease (43.11%) for AgNPs. It is important to note that after coupling with the nanosheets, the toxicity efficiency of AgNPs was increased by nearly three times at the same concentration and the GO nanosheets also enhanced the antifungal activity by 7-fold. In the case of GO sheets alone, almost no inhibition of spore growth was shown even at 7.81 μg/mL and the germination rate was up to 87.2%, which can be observed in the corresponding microscopy images of *F. graminearum* spore germination (Figures S4 and S5). Actually, the significant growth inhibition toward spores was observed at 50 μg/mL, a concentration much higher than that of AgNPs or GO-AgNPs nanocomposite. The corresponding microscopy images of *F. graminearum* spore germination in the presence of GO-AgNPs nanocomposite were taken by Leica (Germany, DCF425) (Figure 6). For the spores without any nanomaterials, normal and long germ tubes could be seen growing from the top of spores. However, for the spores treated with the GO-AgNPs nanocomposite, the spore germ tube was strongly inhibited and the intensity of the inhibitory action was concentration-dependent (Figure S6).

Additionally, we performed an inactivation experiment to evaluate the sporicidal activities of the GO-AgNPs composite. As shown in Table 1, the MFC of GO-AgNPs composite and AgNPs was determined to be 9.37 and 12.45 μg/mL, respectively, at which nearly all the cells were killed by the nanoparticles. However, the MFC of pure GO nanosheets was as high as 500 μg/mL. While both of them exerted significant inhibition of spore germination at 4.68 μg/mL, GO-AgNPs nanocomposite could completely kill cells under a lower concentration, which also suggested that GO-AgNPs composite had stronger antifungal activity. In this sense, GO-AgNPs hybrids had an obvious increment effect in antimicrobial activity over pure AgNPs or GO sheets. The vital reason for this is the enhancement of the dispersion state of the AgNPs

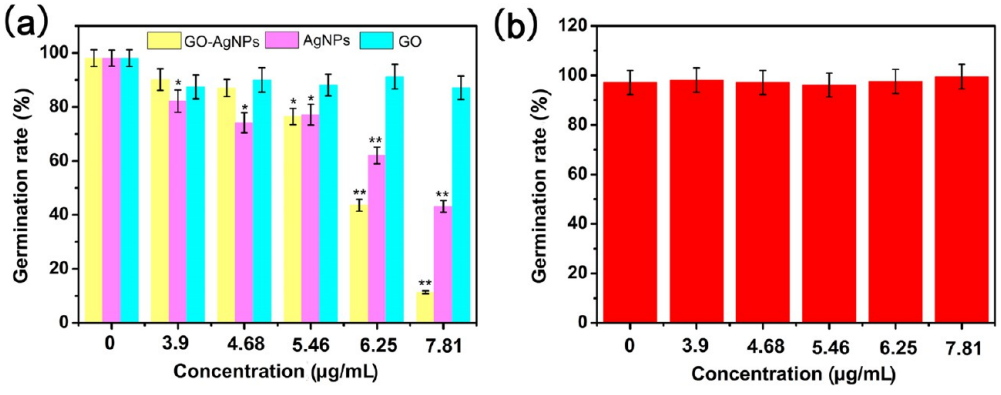

Figure 5. Dose−response of germination rate of *F. graminearum* spores. (a) The germination rates of spores treated with GO, AgNPs, and GO-AgNPs nanocomposite. (b) PVP in the concentration range of 3.9 to 7.81 μg/mL.

DOI: 10.1021/acsami.6b05730
ACS Appl. Mater. Interfaces 2016, 8, 24057−24070

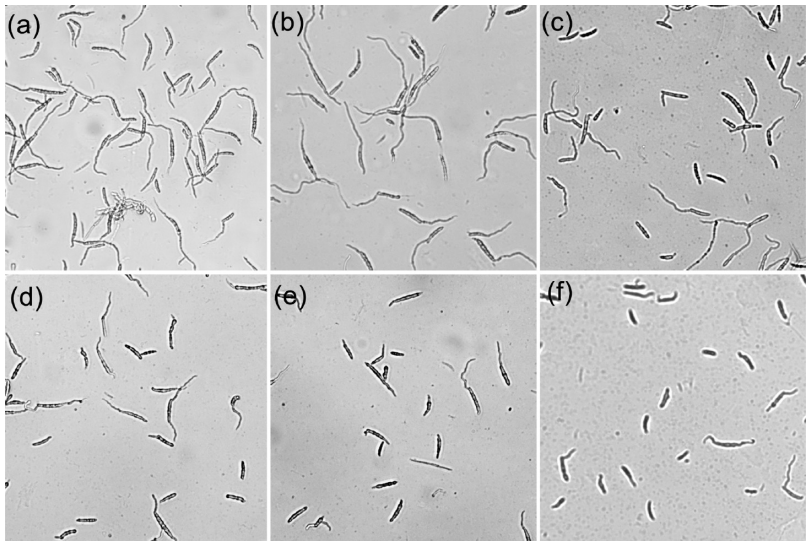

Figure 6. Photomicrographs of *F. graminearum* macroconidial germination after exposure to 0, 3.91, 4.68, 5.46, 6.25, and 7.81 μg/mL of GO-AgNPs nanocomposite separately. *F.graminearum* conidia were germinated on coverslips for 7 h at 28 °C (a) without (the control) and (b–f) with GO-AgNPs nanocomposite at different concentrations.

nanoparticle. Nanoparticles interact with biological cells mainly depending on their surface properties, agglomeration state.[20] It is well-known that the agglomeration liability in solution of AgNPs caused by the strong van der Waals interaction among these silver nanoparticles restricts their antibacterial action.[14,17] After stabilization with GO sheets, the nanocomposites had higher zeta-potentials in pure water to induce stable dispersions.[42] Upon contact with fungal spores or mycelia, GO sheets can act as bridges to bind silver nanoparticles homogeneously to promote the direct contact between Ag nanoparticles and cells, suggesting the synergistic effect of GO sheets and AgNPs, which played an important role in the antibacterial activity of AgNPs by inducing significant antifungal activity of the nanocomposite.[50] The well-known toxicity mechanisms proposed are that catalytic oxidation by metallic silver and the release of dissolved monovalent silver ion probably contribute to the bactericidal effects of silver particles.[17,51]

Silver ions released from silver nanoparticles on the surface of GO sheets were detected in dialysis experiments. As shown in Figure S7, the content of Ag^+ diffused out of the dialysis tube was increased in 20 days and finally, only 89.7% Ag^+ was released (Figure S7). The release of Ag^+ favored the high antimicrobial activity, especially the slow and long release of Ag^+. The released silver ions can strongly interact with thiol, carboxyl, hydroxyl, amino, phosphate, and imidazole groups in proteins and enzymes on bacterial membranes which may complicate the mechanistic understanding of the prohibition on the bacterial growth.[51]

Additionally, as shown in Figure 4, XPS spectrum of GO-AgNPs showed that the peak of oxygen-containing functional groups was significantly deceased in comparison to GO sheets, which was attributed to the reduction reaction. After incubation with *F. graminearum* spores, the XPS spectrum of GO-AgNPs was redetermined and interestingly, the results indicated that the peak area ratios of the C−OH and C═O bonds to the C−C bonds deceased greatly by 33.84 and 57.14% respectively when in contact with fungal spores for 24 h (Figure S8). It seems that the fungal spores induced further chemical reduction, thus reducing the intensity of oxygen-containing functional groups. Currently, there is much interest in the green synthetic procedures for nanoparticles by biological systems due to the reduction ability during their biochemical process.[52,53] It was worth noting that GO, with excellent electrical properties, can act as a terminal electron acceptor for metal-reducing and some environmental bacteria.[52] Among them, prokaryotic bacteria can play a most efficient role in the chemical reduction of GO sheets, such as *Shewanella* bacterium and *E. coli*, through transferring metabolically generated electrons in their glycolysis process from the cell interior to GO as an external electron acceptor.[54,55] Our results displayed that electron transfer between the reduced GO and fungal cell was contributed to the high antibacterial activity, possibly by changing the membrane electric potential and inducing cell growth inhibition, even lethal effects, as reported by Chen et al.[10]

3.3. Hyphal Structure Change Induced by GO-AgNPs Nanocomposite. As demonstrated above, GO-AgNPs nanocomposite significantly restrained the germination of spores and the development of germ tubes; thus, the mycelia grown from spores are assumed to be affected by the treatment of GO-AgNPs nanocomposite. To find out the interaction and the mechanism by which GO-AgNPs nanomaterials influence the growth of *F. graminearum*, optical microscopy and SEM analyses were performed to examine the structural changes of fungal samples. After 3 days of growth on normal PDA media at 30 °C, the hyphae were sprayed with GO-AgNPs nanocomposite dispersion, and the untreated and treated samples were viewed under a SEM (JEOL JSM-6700F). The hyphae of control group (treated with water) in Figure 7a appeared smooth and remained intact after incubation, with slender bodies, whereas, after contact with 6.85 and 7.81 μg/mL GO-AgNPs composite, the hyphae became sunken and stacked together (Figures 7b and Figure 7c). Additionally, some old hyphae were obviously deformed and bulked (Figure 7e). Figure 7f shows a representative collapsed structure of *F. graminearum* in the presence of GO-AgNPs nanocomposite, along with distortion.

The well-known toxicity mechanisms proposed are that catalytic oxidation by metallic silver and the release of dissolved

DOI: 10.1021/acsami.6b05730
ACS Appl. Mater. Interfaces 2016, 8, 24057−24070

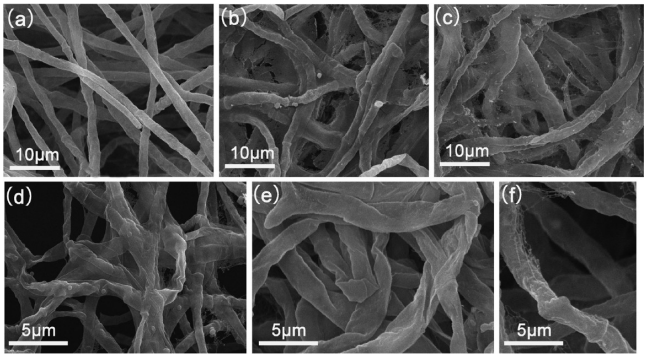

Figure 7. SEM images of *F. graminearum* hyphae in the presence of water (a) and 6.25 (b) and 7.81 μg/mL (c) of GO-AgNPs nanocomposite. (d–f) The typical structure of old hyphae and normal hyphae after treatment with 7.81 μg/mL of GO-AgNPs nanocomposite.

monovalent silver ion probably contribute to the bactericidal effects of silver particle.[17] The released silver ions can strongly interact with thiol, carboxyl, hydroxyl, amino, phosphate, and imidazole groups in proteins and enzymes on bacterial membranes, which may complicate the mechanistic understanding of the prohibition on the bacterial growth.[56] Ag^+ released from silver nanoparticles on the surface of GO sheets was detected in dialysis experiments. As shown in Figure S7, the content of Ag^+ diffused out of the dialysis tube was increased in 10 days and finally, only 89.7% Ag^+ was released. The release of Ag^+ favored the high antimicrobial activity, especially the slow and long release of Ag^+.

3.4. Spore Cell Observation by SEM and TEM after Treatment with GO-AgNPs Nanocomposite. The scanning electron microscopy (SEM) and TEM are widely used to assess the direct interactions between the biological cells and nanomaterials.[10] To investigate the changes in the cellular morphologies of the treated *F. graminearum* spores, microscopy imaging experiments were conducted. From Figure 7a, it can be seen that, as part of phragmospore, all the macroconidia under untreated conditions displayed the typical slender, sickle-shape morphology and possessed an intact and plump structure with three transverse septa. However, after direct contact with GO-AgNPs nanocomposite for 2 h, most of the *F. graminearum* macroconidia were crumpled, wizened, and obviously stacked together with nanomaterials, which probably facilitated the direct contact of Ag nanoparticles on the surface of GO nanosheets with the cells. In addition, the regular cell construction disappeared, and macroconidia seemed to be heavily damaged, indicating the significant effect of the nanocomposite on the spores (Figure 8b). These findings were similar to a previous report showing that the adsorption of nanoparticles to the bacterial cell walls is responsible for their bactericidal effects from the construction of nanomaterials and biological cells, and the abundant oxygenated groups of GO can develop hydrogen bonds to interact with the lipopolysaccharide subunits of the cell membranes which contain sugars, phosphates, and lipids.[57]

The toxicity action was also investigated by TEM imaging. Figure 9a shows the normal spores with well-defined and integrated cell membranes which contained a number of tiny organelles. However, once the spores were mixed with nanomaterials, the GO nanosheets loaded with silver nanoparticles were wrapped around the cell walls of spores,

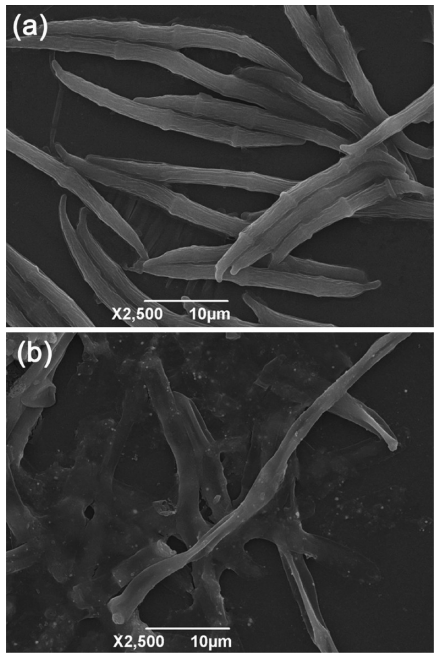

Figure 8. SEM images of conidia of *F. graminearum* after incubation with sterile water (a) and GO-AgNPs nanocomposite (b) for 3 h.

hindering their nutrient absorption and transport from external environment.[58] To date, there have been various reports about the possible antibacterial mechanisms of graphene-based nanomaterials, including cell membrane stress induced by the mechanical injury of graphene nanosheets and oxidative stress associated with the generation of cellular ROS.[59] Akhavan et al. have confirmed that graphene oxide nanowalls with extremely sharp edges exhibited toxicity on bacteria, causing physical membrane damage.[60] Oxidative cell damage was also proposed as one of the main mechanisms for the cytotoxicity of silver nanoparticles on cells and bacteria.[61] As shown in Figure 9, the high surface area of GO sheets facilitated the contact of silver nanoparticles with cells, which was consistent with SEM imaging experiments. The blue arrows indicated the direct interaction of AgNPs on the surface of GO nanosheets with the outer membrane of spores (Figure 9b, c). There is no doubt that the synergistic effect of GO-AgNPs hybrids was responsible for the remarkable antifungal action of the synthesized composite toward fungal spores and hyphae.

Collectively, the direct-contact interaction of GO-AgNPs nanocomposite with cells greatly enhanced the toxicity action, possibly by causing both physical and chemical injuries, not only due to the extremely sharp edges of graphene nanowalls and silver nanoparticles, but also the release of Ag^+ on the surface of AgNPs. There is no doubt that the synergistic effect of GO-AgNPs hybrids was responsible for the remarkable antifungal action of the synthesized composite toward fungal spores and hyphae.

Meanwhile, the relatively high stability of AgNPs dispersion from the use of GO sheets cannot be ignored. When compared to AgNPs alone, GO-AgNPs nanocomposites exhibited much stronger antifugal activities. The difference between them appears attributed to the phase behavior and biodistribution of nanoparticles, which play a vital role when nanoparticles interact with biological systems.[20] It should be noted that GO sheets help the AgNPs to stick or transport to a place where they can be better delivered to the fungus. This formation

DOI: 10.1021/acsami.6b05730
ACS Appl. Mater. Interfaces 2016, 8, 24057–24070

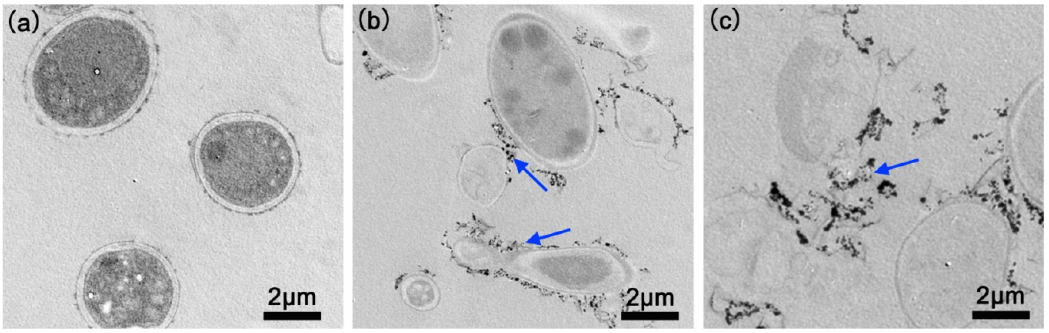

Figure 9. TEM images of conidia of *F. graminearum* after incubation with sterile water (a) and GO-AgNPs nanocomposite (b, c) for 3 h.

pattern, for one thing, contributes to the stable dispersion of the nanoparticles, and extremly affects their antibacterial activity. On the other hand, it may particularly affect silver excretion and result in long residence time during the interation of nanoparticles with the biological cells.[13,20] Ultimately, the nanocomposites preponderantly inhibited the spore germination and even killed the spore, leading to hyphal impairment and even the complete inhibition of sporulation.

3.5. ROS Production. The aforementioned results indicated that physical damage on the hyphae and spores was obviously associated with the memchanism of GO-AgNPs. As far as we know, the toxicity action mediated by oxidative stress on the biological cells commonly occurred under the treatment of the biological cells with various nanomaterials, such as metal oxide nanoparticles and carbon nanomaterials.[59−62] Hence, the production of ROS was further detected to evaluate the antifungal activity of GO-AgNPs. ROS are a group of short-lived reactive oxidants, including the superoxide radical, hydroxyl radical (−OH), hydrogen peroxide (H_2O_2), singlet oxygen, etc.[59] The ROS level of cells was measured after incubation separately with a different conceatration of GO, AgNPs and GO-AgNPs. As shown in Figure 10, GO, AgNPs,

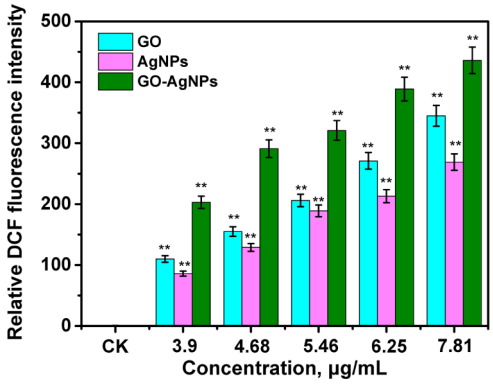

Figure 10. ROS level of *F. graminearum* spore after incubation with different concentrations of GO, AgNPs, and GO-AgNPs nanocomposite.

and GO-AgNPs induced a significant concentration-dependent increase in ROS production. It should be noted that, despite ROS induction for all the particles, GO-AgNPs showed a relatively higher level than the other two. The ROS level for GO sheets and AgNPs at 7.81 μg/mL was 151- and 271-fold that of the control, while the content of Ag ion showed a 437-fold increase in the presence of GO-AgNPs composite, reflecting a synergetic effect. It seems that oxdation stress excactly makes a great contribution to the strong anfungal activity of the GO-AgNPs composite. ROS are normal and harmless byproducts in the aerobic metabolism process, but biological cells would cause excessive ROS generation under adverse conditions.[62] The excessive ROS would induce injury to various cellular constituents such as lipids, proteins and DNA, influence various signaling pathways, and finally result in growth arrest or cell death.[62] These results suggested that, when in contact with fungal spores, GO-AgNPs not only result in obvious morphological injury but also induce ROS production to initiate fungal spore inhibition and death.

3.6. Detached Leaf Experiment for Controlling Fungal Disease. Nanomaterials have shown great promise for their application in plant protection and nutrition due to their size-dependent qualities, high surface-to-volume ratio and unique optical properties.[63] The results from this study have demonstrated that GO-AgNPs nanocomposite could not only partly inhibit the sporulation process but also have sporicidal action to destroy the hyphal structure. The unique antifungal activity of GO-AgNPs nanocomposite at such a low concentration (4.68 μg/mL) may have the potential for controlling the plant disease in the future. Therefore, we performed the detached leaf experiment to further investigate whether the GO-AgNPs nanocomposite can protect crop from *F. graminearum* invasion as an antibacterial agent. Experiments with detached leaf segments are frequently employed in bacterial and fungal pathogen disease tests, such as *Stagonospora nodorum*,[64] *Septoria tritici*,[65] *Erysiphe graminis DC. f.sp. avenae*,[66] and *Microdochium nivale*.[67] Back in 1999, the study of H. Diamond et al. supported that *Fusarium* ear blight (FEB) disease measurements of wheat cultivars tested in the detached leaf experiments were significantly correlated with the results obtained from the glasshouse whole plant study.[38] In this study, a leaf detached from a 3-week-old wheat seedling was used for the experiment, with the same plant age and positioned leaves. After spraying GO-AgNPs nanocomposite on the wheat leaves, the leaf spot disease or the lesion size was significantly reduced compared to the untreated control, although some small-size spots were observed (Figure 11). This observation sheds light on our previous finding that carbon-based nanomaterials displayed high antimicrobial action toward phytopahtogens and could be applied in plant management.[10] However, scholars vary in their views about the potential application of graphene, especially the cytotoxic effects or biocompatibility of graphene in the biological system. Several studies indicated that graphene and AgNPs exerted mild cytotoxicity toward mammalian cells and could be applied for medical disinfection.[68] Conversely, Akhavan et al. reported the effects of nanoscale graphene oxide (NGO) sheets on the reproduction

DOI: 10.1021/acsami.6b05730
ACS Appl. Mater. Interfaces 2016, 8, 24057−24070

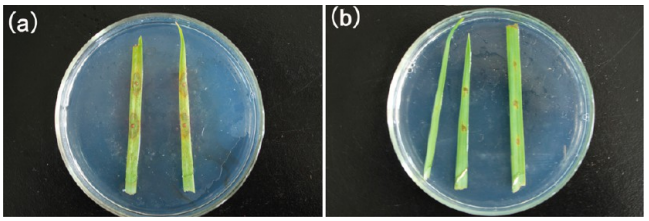

Figure 11. Detached wheat leaves treated with (a) sterile deionized water and (b) GO-AgNPs nanocomposite. Three plants were tested for each treatment and all the experiments were performed in triplicate.

capability of Balb/C mice at the intravenous injection concentration ≥200 mg/mL in vivo.[69] They found that NGO sheets were absorbed in testis and induced remarkable DNA damage and chromosomal aberration. Additionally, the hormone secretion and pregnant functionality was also disturbed. It should be noted that, in the present experiment, the inhibitory concentration was only up to 4.68 μg/mL, which is extremly lower than the previously reported toxicity dose on plant and mammalian cells.[20] For this reason, GO-AgNPs may have the potential application in crop disease mangement, but a consistent aim of agriculture is the sustainable development or management of natural resources. Therefore, the nanomaterials

Table 2. Several Currently Used Chemical Fungicides against *Fusarium sps.*

chemical fungicide	*Fusarium* strains	effective concentration (μg/mL)	experimental method	reference
GO-AgNPs	*F. graminearum*	9.37	in vitro, LC inhibit mycelia	in this experiment
hymexarizonaol	*F. graminearum*	62.5	in vitro, EC_{50} germination inhibition	in this experiment
acibenzolar-*S*-methyl	*Fusarium wilt*	50	greenhouse test	Elmer et al.[71]
prothioconazole	*F. avenaceum*	0.27	in vitro, ED_{50} inhibit mycelia	Müllenborn et al.[72]
	F.crookwellense	3.2		
	F. culmorum	0.19		
	F. graminearum	0.4		
	F. poae	0.09		
	F.sporotrichioides	0.23		
tebuconazole	*F. avenaceum*	1.7	in vitro, $ED_{50/90}$ inhibit mycelia	Müllenborn et al.,[72] Marín et al.[73]
	F. crookwellense	6.5		
	F. culmorum	2.1		
	F. graminearum	0.57		
	F. poae	1.5		
	F. sporotrichioides	0.24		
	F.verticillioides	3.50		
	F.proliferatum	10.0		
azoxystrobin	*F. avenaceum*	69	In vitro, ED50 Inhibit mycelia	Müllenborn et al.[72]
	F. crookwellense	>100		
	F. culmorum	>100		
	F. graminearum	>100		
	F. poae	>100		
	F. sporotrichioides	>100		
fluoxastrobin	*F. avenaceum*	43	in vitro, ED_{50} inhibit mycelia	Müllenborn et al.[72]
	F. crookwellense	>100		
	F. culmorum	64		
	F. graminearum	>100		
	F. poae	>100		
	F. sporotrichioides	>100		
prochloraz	*F. oxysporum f. sp. cubense*	1	in vitro, LC completely inhibit mycelia	Nel et al.[74]
propiconazole	*F. oxysporum f.sp. cubense*	10	in vitro, LC completely inhibit mycelia	Nel et al.[74]
cyproconazole/propiconazole	*F. oxysporum f.sp. cubense*	100	in vitro, LC completely inhibit mycelia	Nel et al.[74]
phosphorous acid	*F. oxysporum f.sp. cubense*	>100	in vitro, LC completely inhibit mycelia	Nel et al.[74]
azoxystrobin	*F. oxysporum f.sp. cubense*	250	glasshouse test control *Fusarium* wilt	Gullino et al.[75]
kresoxim-methyl	*F. oxysporum f.sp. cubense*	250	glasshouse test control *Fusarium* wilt	
copper oxychloride	*F. oxysporum f.sp. cubense*	>100	in vitro, LC completely inhibit mycelia	Nel et al.[74]
carbendazim	*F. oxysporum Klotz*	0.235	in vitro, EC_{50} inhibit mycelia	Song et al.[76]
toclofos-methyl	*F. oxysporum Klotz*	53.606	in vitro, EC_{50} inhibit mycelia	Song et al.[76]
hymexazol	*F. oxysporum Klotz*	69.961	in vitro, EC_{50} inhibit mycelia	Song et al.[76]
azoxystrobin	*F. oxysporum Klotz*	144.58	in vitro, EC_{50} inhibit mycelia	Song et al.[76]
carboxin	*F. oxysporum Klotz*	154.0	in vitro, EC_{50} inhibit mycelia	Song et al.[76]

DOI: 10.1021/acsami.6b05730
ACS Appl. Mater. Interfaces 2016, 8, 24057−24070

should be further evaluated to guarantee their safe use in agriculture.

In Table 2, we provided reference data on currently used chemicals against this *Fusarium sps*. Additionally, we chose one commercial fungicide (Hymexarizonaol) to compare its antifungal activity on *F. graminearum* with that of the GO-AgNPs and the reference data. The results showed that Hymexarizonaol could completely kill the spores at a concentration of 62.5 μg/mL, far higher than that of GO-AgNPs. As shown in Table 2, all the chemical fungicides exhibited their antifungal activity at a different effective concentration, including lethal concentration (LC), with 50% effective dose indicated as ED50 and the concentration for 50% of maximal effect as EC50. Compared with the currently used chemical fungicides against *Fusarium* in agriculture (Table 2), it can be seen that, except for prothioconazole, tebuconazole and prochloraz, the lethal concentration of the GO-AgNPs nanocomposite (9.37 μg/mL) is much lower than that of the other fungicides in previous studies. Particularly, its antifungal activity against *F. graminearum* is several times higher than that of azoxystrobin, fluoxastrobin, carboxin and azoxystrobin, whose 50% effective doses are all nearly more than 100 μg/mL. The unique antifungal activity of GO-AgNPs nanocomposite at such a low MIC and MFC (4.68 and 9.37 μg/mL) suggests its great potential for controlling the plant disease in the future. More importantly, Lu et al. have reported that nanoparticles were not genotoxic or cytotoxic to humans.[14] Recently, Tan's group has demonstrated that there was no visual phytotoxicity on leaves when 100 ppm of Ag@dsDNA@GO was applied on the tomato transplants in a greenhouse experiment, and when compared to the untreated control, the nanoparticles can significantly reduce the severity of bacterial spot caused by *Xanthomonas perforans*.[70] GO-AgNPs nanocomposite, as a novel bactericide, may well meet the requirements of plant disease control, whose aim is to hinder the development of pathogens efficiently and create a sustainable balance between complementary approaches and field management. However, further research should be conducted about the phytotoxic behavior of the nanomaterials before use under field conditions.

4. CONCLUSIONS

In this study, we have fabricated GO-AgNPs nanocomposite through the interfacial electrostatic self-assembly method and characterized its properties using various technical devices. The as-prepared GO-AgNPs nanocomposite exhibits good dispersibility in water without any further modification. The toxicity action of the synthesized GO-AgNPs nanocomposite on *F. graminearum* was investigated for the first time. The GO-AgNPs nanocomposite shows enhanced antimicrobial activity at an exceedingly low concentration (9.37 μg/mL) compared to the pure AgNPs (12.45 μg/mL) and GO nanosheets (250 μg/mL), which may prevent the supererogatory effect on the host plant. Results from SEM, TEM and ROS analyses indicate that the synergy of both GO sheets and AgNPs plays a vital role in their inactivation effects, not only inducing physical damage on biological structure, but also causing oxidation stress on cells. The detached leaf experiment has confirmed that the nanocomposite can significantly control the development of the leaf spot caused by *F. graminearum* spore, and protect plants from pathogen infection. The overall findings from this study suggest that the unique shape and ultrasmall size of GO-AgNPs nanocomposite make it a promising antimicrobial agent for preventing crop diseases caused by fungal or bacterial pathogens.

■ ASSOCIATED CONTENT

Supporting Information

The Supporting Information is available free of charge on the ACS Publications website at DOI: 10.1021/acsami.6b05730.

Germination rate of spores treated with PDDA (Figure S1); photomicrographs of macroconidial germination after treatment with GO sheets, AgNPs, and GO-AgNPs (Figure S2−S4); germ tube length of the *F. graminearum* conidium after treatment with GO-AgNPs (Figure S5); Ag^+ release of GO-AgNPs nanocomposite during 20 days (Figure S6); and peak area relative ratios of oxygen-containing functional groups to the C−C bonds (Figure S7) (PDF)

■ AUTHOR INFORMATION

Corresponding Author

*Tel: +86-27-87288505. Fax: +86-27-87288505. E-mail: hyhan@mail.hzau.edu.cn.

Notes

The authors declare no competing financial interest.

■ ACKNOWLEDGMENTS

The authors gratefully acknowledge the financial support for this research from National Natural Science Foundation of China (21375043, 21175051).

■ REFERENCES

(1) Goswami, R. S.; Kistler, H. C. Heading for Disaster: *Fusarium graminearum* on Cereal Crops. *Mol. Plant Pathol.* **2004**, *5*, 515−525.
(2) Clear, R.; Patrick, S.; Gaba, D. Prevalence of Fungi and Fusariotoxins on Barley Seed from Western Canada, 1995 to 1997. *Can. J. Plant Pathol.* **2000**, *22*, 44−50.
(3) Lemanceau, P.; Alabouvette, C. Biological Control of Fusarium Diseases by Fluorescent Pseudomonas and Non-pathogenic Fusarium. *Crop Prot.* **1991**, *10*, 279−286.
(4) Zasloff, M. Antimicrobial Peptides of Multicellular Organisms. *Nature* **2002**, *415*, 389−395.
(5) Gao, A. G.; Hakimi, S. M.; Mittanck, C. A.; Wu, Y.; Woerner, B. M.; Stark, D. M.; Shah, D. M.; Liang, J.; Rommens, C. M. Fungal Pathogen Protection in Potato by Expression of A Plant Defensin Peptide. *Nat. Biotechnol.* **2000**, *18*, 1307−1310.
(6) Zhang, P.; Cui, H.; Zhong, X.; Li, L. Effects of Nano-TiO_2 Semiconductor Sol on Prevention from Plant Diseases. *Nanoscience* **2007**, *12*, 1−6.
(7) Jo, Y. K.; Kim, B. H.; Jung, G. Antifungal Activity of Silver Ions and Nanoparticles on Phytopathogenic Fungi. *Plant Dis.* **2009**, *93*, 1037−1043.
(8) Lamsal, K.; Kim, S. W.; Jung, J. H.; Kim, Y. S.; Kim, K. S.; Lee, Y. S. Application of Silver Nanoparticles for the Control of *Colletotrichum* Species In Vitro and Pepper Anthracnose Disease in Field. *Mycobiology* **2011**, *39*, 194−199.
(9) Chen, J.; Wang, X.; Han, H. A New Function of Graphene Oxide Emerges: Inactivating Phytopathogenic Bacterium *Xanthomonas oryzae pv. Oryzae*. *J. Nanopart. Res.* **2013**, *15*, 1658.
(10) Chen, J.; Peng, H.; Wang, X.; Shao, F.; Yuan, Z.; Han, H. Graphene Oxide Exhibits Broad-spectrum Antimicrobial Activity against Bacterial Phytopathogens and Fungal Conidia by Intertwining and Membrane Perturbation. *Nanoscale* **2014**, *6*, 1879−1889.
(11) Zhao, X.; Liu, R. Recent Progress and Perspectives on the Toxicity of Carbon Nanotubes at Organism, Organ, Cell, and Biomacromolecule Levels. *Environ. Int.* **2012**, *40*, 244−255.

DOI: 10.1021/acsami.6b05730
ACS Appl. Mater. Interfaces 2016, 8, 24057−24070

(12) Gosheger, G.; Hardes, J.; Ahrens, H.; Streitburger, A.; Buerger, H.; Erren, M.; Gunsel, A.; Kemper, F. H.; Winkelmann, W.; von Eiff, C. Silver-coated Megaendoprostheses in a Rabbit Model—an Analysis of the Infection Rate and Toxicological Side Effects. *Biomaterials* **2004**, *25*, 5547−5556.
(13) Li, C.; Wang, X.; Chen, F.; Zhang, C.; Zhi, X.; Wang, K.; Cui, D. The Antifungal Activity of Graphene Oxide-silver Nanocomposites. *Biomaterials* **2013**, *34*, 3882−3890.
(14) Lu, W.; Senapati, D.; Wang, S.; Tovmachenko, O.; Singh, A. K.; Yu, H.; Ray, P. C. Effect of Surface Coating on the Toxicity of Silver Nanomaterials on Human Skin Keratinocytes. *Chem. Phys. Lett.* **2010**, *487*, 92−96.
(15) Yen, H. J.; Hsu, S. h.; Tsai, C. L. Cytotoxicity and Immunological Response of Gold and Silver Nanoparticles of Different Sizes. *Small* **2009**, *5*, 1553−1561.
(16) Pal, S.; Tak, Y. K.; Song, J. M. Does the Antibacterial Activity of Silver Nanoparticles Depend on the Shape of the Nanoparticle? A Study of the Gram-Negative Bacterium *Escherichia coli*. *Appl. Environ. Microbiol.* **2007**, *73*, 1712−1720.
(17) Xiong, Y.; Brunson, M.; Huh, J.; Huang, A.; Coster, A.; Wendt, K.; Fay, J.; Qin, D. The Role of Surface Chemistry on the Toxicity of Ag Nanoparticles. *Small* **2013**, *9*, 2628−2638.
(18) Zhang, H.; Smith, J. A.; Oyanedel-Craver, V. The Effect of Natural Water Conditions on the Anti-bacterial Performance and Stability of Silver Nanoparticles Capped with Different Polymers. *Water Res.* **2012**, *46*, 691−699.
(19) El Badawy, A. M.; Silva, R. G.; Morris, B.; Scheckel, K. G.; Suidan, M. T.; Tolaymat, T. M. Surface Charge-dependent Toxicity of Silver Nanoparticles. *Environ. Sci. Technol.* **2011**, *45*, 283−287.
(20) Stark, W. J. Nanoparticles in Biological Systems. *Angew. Chem., Int. Ed.* **2011**, *50*, 1242−1258.
(21) Chen, M.; Wang, L. Y.; Han, J. T.; Zhang, J. Y.; Li, Z. Y.; Qian, D. J. Preparation and Study of Polyacryamide-stabilized Silver Nanoparticles Through a One-pot Process. *J. Phys. Chem. B* **2006**, *110*, 11224−11231.
(22) Lv, M.; Su, S.; He, Y.; Huang, Q.; Hu, W.; Li, D.; Fan, C.; Lee, S. T. Long-Term Antimicrobial Effect of Silicon Nanowires Decorated with Silver Nanoparticles. *Adv. Mater.* **2010**, *22*, 5463−5467.
(23) Eda, G.; Fanchini, G.; Chhowalla, M. Large-area Ultrathin Films of Reduced Graphene Oxide as a Transparent and Flexible Electronic Material. *Nat. Nanotechnol.* **2008**, *3*, 270−274.
(24) Li, D.; Müller, M. B.; Gilje, S.; Kaner, R. B.; Wallace, G. G. Processable Aqueous Dispersions of Graphene Nanosheets. *Nat. Nanotechnol.* **2008**, *3*, 101−105.
(25) Premkumar, T.; Geckeler, K. E. Graphene−DNA Hybrid Materials: Assembly, Applications, and Prospects. *Prog. Polym. Sci.* **2012**, *37*, 515−529.
(26) Chowdhury, I.; Duch, M. C.; Mansukhani, N.; Hersam, M. C.; Bouchard, D. Interactions of Graphene Oxide Nanomaterials with Natural Organic Matter and Metal Oxide Surfaces. *Environ. Sci. Technol.* **2014**, *48*, 9382−9390.
(27) Lin, Y.; Jin, J.; Song, M. Preparation and Characterisation of Covalent Polymer Functionalized Graphene Oxide. *J. Mater. Chem.* **2011**, *21*, 3455−3461.
(28) Bai, S.; Shen, X. Graphene−inorganic Nanocomposites. *RSC Adv.* **2012**, *2*, 64−98.
(29) Akhavan, O.; Ghaderi, E. Photocatalytic Reduction of Graphene Oxide Nanosheets on TiO_2 Thin Film for Photoinactivation of Bacteria in Solar Light Irradiation. *J. Phys. Chem. C* **2009**, *113*, 20214−20220.
(30) Akhavan, O.; Choobtashani, M.; Ghaderi, E. Protein Degradation and RNA Efflux of Viruses Photocatalyzed by Graphene-Tungsten Oxide Composite Under Visible Light Irradiation. *J. Phys. Chem. C* **2012**, *116*, 9653−9659.
(31) Hu, C.; Liu, Y.; Qin, J.; Nie, G.; Lei, B.; Xiao, Y.; Zheng, M.; Rong, J. Fabrication of Reduced Graphene Oxide and Sliver Nanoparticle Hybrids for Raman Detection of Absorbed Folic Acid: a Potential Cancer Diagnostic Probe. *ACS Appl. Mater. Interfaces* **2013**, *5*, 4760−4768.
(32) Das, M. R.; Sarma, R. K.; Borah, S. C.; Kumari, R.; Saikia, R.; Deshmukh, A. B.; Shelke, M. V.; Sengupta, P.; Szunerits, S.; Boukherroub, R. The Synthesis of Citrate-modified SilverNanoparticles in an Aqueous Suspension of Graphene Oxide Nanosheets and Their Antibacterial Activity. *Colloids Surf., B* **2013**, *105*, 128−136.
(33) Ouda, S. M. Antifungal Activity of Silver and Copper Nanoparticles on Two Plant Pathogens, *Alternaria alternata* and *Botrytis cinerea*. *Res. J. Microbiol.* **2014**, *9*, 34−42.
(34) Hummers, W. S., Jr; Offeman, R. E. Preparation of Graphitic Oxide. *J. Am. Chem. Soc.* **1958**, *80*, 1339−1339.
(35) Lee, P.; Meisel, D. Adsorption and Surface-enhanced Raman of Dyes on Silver and Gold Sols. *J. Phys. Chem.* **1982**, *86*, 3391−3395.
(36) Ren, W.; Fang, Y.; Wang, E. A Binary Functional Substrate for Enrichment and Ultrasensitive SERS Spectroscopic Detection of Folic Acid Using Graphene Oxide/Ag Nanoparticle Hybrids. *ACS Nano* **2011**, *5*, 6425−6433.
(37) Seong, K. Y.; Zhao, X.; Xu, J. R.; Güldener, U.; Kistler, H. C. Conidial Germination in the Filamentous Fungus *Fusarium graminearum*. *Fungal Genet. Biol.* **2008**, *45*, 389−399.
(38) Diamond, H.; Cooke, B. Towards the Development of a Novel in Vitro Strategy for Early Screening of Fusarium Ear Blight Resistance in Adult Winter Wheat Plants. *Eur. J. Plant Pathol.* **1999**, *105*, 363−372.
(39) Lorito, M.; Woo, S. L.; Fernandez, I. G.; Colucci, G.; Harman, G. E.; Pintor-Toro, J. A.; Filippone, E.; Muccifora, S.; Lawrence, C. B.; Zoina, A.; et al. Genes from Mycoparasitic Fungi as a Source for Improving Plant Resistance to Fungal Pathogens. *Proc. Natl. Acad. Sci. U. S. A.* **1998**, *95*, 7860−7865.
(40) Badawy, A. M. E.; Luxton, T. P.; Silva, R. G.; Scheckel, K. G.; Suidan, M. T.; Tolaymat, T. M. Impact of Environmental Conditions (pH, ionic strength, and electrolyte type) on the Surface Charge and Aggregation of Silver Nanoparticles Suspensions. *Environ. Sci. Technol.* **2010**, *44*, 1260−1266.
(41) Xu, C.; Wang, X.; Zhu, J. Graphene-metal Particle Nanocomposites. *J. Phys. Chem. C* **2008**, *112*, 19841−19845.
(42) Luechinger, N. A.; Booth, N.; Heness, G.; Bandyopadhyay, S.; Grass, R. N.; Stark, W. J. Melt-Processable Metal-Polymer Hybrid Materials: Use of Graphene as a Dispersing Agent. *Adv. Mater.* **2008**, *20*, 3044−3049.
(43) Xu, C.; Wang, X. Fabrication of Flexible Metal-Nanoparticle Films Using Graphene Oxide Sheets as Substrates. *Small* **2009**, *5*, 2212−2217.
(44) de Faria, A. F.; Martinez, D. S. T.; Meira, S. M. M.; de Moraes, A. C. M.; Brandelli, A.; Alves, O. L.; et al. Anti-adhesion and Antibacterial Activity of Silver Nanoparticles Supported on Ggraphene Oxides Sheets. *Colloids Surf., B* **2014**, *113*, 115−124.
(45) Huang, Q.; Wang, J.; Wei, W.; Yan, Q.; Wu, C.; Zhu, X. A Facile and Green Method for Synthesis of Reduced Graphene Oxide/Ag Hybrids as Efficient Surface Enhanced Raman Scattering Platforms. *J. Hazard. Mater.* **2015**, *283*, 123−130.
(46) Calizo, I.; Balandin, A. A.; Bao, W.; Miao, F.; Lau, C. N. Temperature Dependence of the Raman Spectra of Graphene and Graphene Multilayers. *Nano Lett.* **2007**, *7*, 2645−2649.
(47) Akhavan, O. Bacteriorhodopsin as A Superior Substitute for Hydrazine in Chemical Reduction of Single-layer Graphene Oxide Sheets. *Carbon* **2015**, *81*, 158−166.
(48) Zhu, Z. J.; Su, M.; Ma, L.; Ma, L. N.; Liu, D. J.; Wang, Z. X. Preparation of Graphene Oxide-silver NanoparticleNanohybrids with Highly Antibacterial Capability. *Talanta* **2013**, *117*, 449−455.
(49) Akhavan, O.; Ghaderi, E.; Akhavan, A. Size-dependent Genotoxicity of Graphene Nanoplatelets in Human Stem Cells. *Biomaterials* **2012**, *33*, 8017−8025.
(50) Bondarenko, O.; Ivask, A.; Käkinen, A.; Kurvet, I.; Kahru, A. Particle-cell Contact Enhances Antibacterial Activity of Silver-Nanoparticles. *PLoS One* **2013**, *8*, e64060.
(51) Matsumura, Y.; Yoshikata, K.; Kunisaki, S.; Tsuchido, T. Mode of Bactericidal Action of Silver Zeolite and Its Comparison with That of Silver Nitrate. *Appl. Environ. Microbiol.* **2003**, *69*, 4278−4281.

DOI: 10.1021/acsami.6b05730
ACS Appl. Mater. Interfaces 2016, 8, 24057−24070

(52) Salas, E. C.; Sun, Z.; Luttge, A.; Tour, J. M. Reduction of Graphene Oxide via Bacterial Respiration. *ACS Nano* **2010**, *4*, 4852−4856.
(53) Shah, M.; Fawcett, D.; Sharma, S.; Tripathy, S. K.; Poinern, G. E. J. Green Synthesis of Metallic Nanoparticles via Biological Entities. *Materials* **2015**, *8*, 7278−7308.
(54) Akhavan, O.; Ghaderi, E. *Escherichia coli* Bacteria Reduce Graphene Oxide to Bactericidal Graphene in a Self-limiting Manner. *Carbon* **2012**, *50*, 1853−1860.
(55) Akhavan, O.; Ghaderi, E.; Esfandiar, A. Wrapping Bacteria by Graphene Nanosheets for Isolation from Environment, Reactivation by Sonication, and Inactivation by Near-Infrared Irradiation. *J. Phys. Chem. B* **2011**, *115*, 6279−6288.
(56) Gupta, A.; Maynes, M.; Silver, S. Effects of Halides on Plasmid-mediated Silver Resistance in Escherichia coli. *Appl. Environ. Microbiol.* **1998**, *64*, 5042−5045.
(57) Elahifard, M. R.; Rahimnejad, S.; Haghighi, S.; Gholami, M. R. Apatite-coated Ag/AgBr/TiO2 visible-light Photocatalyst for Destruction of Bacteria. *J. Am. Chem. Soc.* **2007**, *129*, 9552−9553.
(58) Ma, J.; Zhang, J.; Xiong, Z.; Yong, Y.; Zhao, X. Preparation, Characterization and Antibacterial Properties of Silver-modified Graphene Oxide. *J. Mater. Chem.* **2011**, *21*, 3350−3352.
(59) Liu, S.; Zeng, T. H.; Hofmann, M.; Burcombe, E.; Wei, J.; Jiang, R.; Kong, J.; Chen, Y. Antibacterial Activity of Graphite, Graphite Oxide, Graphene Oxide, and Reduced Graphene Oxide: Membrane and Oxidative Stress. *ACS Nano* **2011**, *5*, 6971−6980.
(60) Akhavan, O.; Ghaderi, E.; Rahighi, R. Toward Single-DNA Electrochemical Biosensing by Graphene Nanowalls. *ACS Nano* **2012**, *6*, 2904−2916.
(61) Su, H. L.; Chou, C. C.; Hung, D. J.; Lin, S. H.; Pao, I. C.; Lin, J. H.; Huang, F. L.; Dong, R. X.; Lin, J. J. The Disruption of Bacterial Membrane Integrity Through ROS Generation Induced by Nanohybrids of Silver and Clay. *Biomaterials* **2009**, *30*, 5979−5987.
(62) Lee, Y. H.; Cheng, F. Y.; Chiu, H. W.; Tsai, J. C.; Fang, C. Y.; Chen, C. W.; Wang, Y. J. Cytotoxicity, Oxidative Stress, Apoptosis and the Autophagic Effects of Silver Nanoparticles in Mouse Embryonic Fibroblasts. *Biomaterials* **2014**, *35*, 4706−4715.
(63) Khot, L. R.; Sankaran, S.; Maja, J. M.; Ehsani, R.; Schuster, E. W. Applications of Nanomaterials in Agricultural Production and Crop Protection: a Review. *Crop Prot.* **2012**, *35*, 64−70.
(64) Baker, E. A.; Smith, I. Development of resistant and susceptible reactions in wheat on inoculation with Septoria nodorum. *Trans. Br. Mycol. Soc.* **1978**, *71*, 475−482.
(65) Arraiano, L.; Brading, P.; Brown, J. A Detached Seedling Leaf Technique to Study Resistance to *Mycosphaerella graminicola* (*anamorph Septoria tritici*) in Wheat. *Plant Pathol.* **2001**, *50*, 339−346.
(66) Roderick, H.; Clifford, B. Variation in Adult Plant Resistance to Powdery Mildew in Spring Oats Under Field and Laboratory Conditions. *Plant Pathol.* **1995**, *44*, 366−373.
(67) Diamond, H.; Cooke, B. Host Specialisation in *Microdochium nivale* on Cereals. *Cereal Res. Commun.* **1997**, *25*, 533−538.
(68) Yang, X. Y.; Zhang, X. Y.; Liu, Z. F.; Ma, Y. F.; Huang, Y.; Chen, Y. S. High-Efficiency Loading and Controlled Release of Doxorubicin Hydrochloride on Graphene Oxide. *J. Phys. Chem. C* **2008**, *112*, 17554−17558.
(69) Akhavan, O.; Ghaderi, E.; Hashemi, E.; Akbari, E. Dose-dependent Effects of Nanoscale Graphene Oxide on Reproduction Capability of Mammals. *Carbon* **2015**, *95*, 309−317.
(70) Ocsoy, I.; Paret, M. L.; Ocsoy, M. A.; Kunwar, S.; Chen, T.; You, M.; Tan, W. Nanotechnology in Plant Disease Management: DNA-Directed Silver Nanoparticles on Graphene Oxide as an Antibacterial against *Xanthomonas perforans*. *ACS Nano* **2013**, *7*, 8972−8980.
(71) Elmer, W. H. Effects of Acibenzolar-S-methyl on the Suppression of Fusarium wilt of Cyclamen. *Crop Prot.* **2006**, *25*, 671−676.
(72) Müllenborn, C.; Steiner, U.; Ludwig, M.; Oerke, E. C. Effect of Fungicides on the Complex of *Fusarium* species and Saprophytic Fungi Colonizing Wheat Kernels. *Eur. J. Plant Pathol.* **2008**, *120*, 157−166.
(73) Marín, P.; de Ory, A.; Cruz, A.; Magan, N.; González-Jaén, M. T. Potential Effects of Environmental Conditions on the Efficiency of the Antifungal Tebuconazole Controlling *Fusarium Verticillioides* and *Fusarium Proliferatum* Growth Rate and Fumonisin Biosynthesis. *Int. J. Food Microbiol.* **2013**, *165*, 251−258.
(74) Nel, B.; Steinberg, C.; Labuschagne, N.; Viljoen, A. Evaluation of Fungicides and Sterilants for Potential Application in the Management of Fusarium wilt of Banana. *Crop Prot.* **2007**, *26*, 697−705.
(75) Gullino, M. L.; Minuto, A.; Gilardi, G.; Garibaldi, A. Efficacy of Azoxystrobin and Other Strobilurins against Fusarium Wilts of Carnation, Cyclamen and Paris Daisy. *Crop Prot.* **2002**, *21*, 57−61.
(76) Song, W.; Zhou, L.; Yang, C.; Cao, X.; Zhang, L.; Liu, X. Tomato Fusarium wilt and Its Chemical Control Strategies in a Hydroponic System. *Crop Prot.* **2004**, *23*, 243−247.

DOI: 10.1021/acsami.6b05730
ACS Appl. Mater. Interfaces 2016, 8, 24057−24070